

Review

# Designs of Anode-Free Lithium-Ion Batteries

Pei Zhao<sup>1</sup>, Jun Pan<sup>2</sup>, Dongqi Zhang<sup>3</sup>, Yufeng Tang<sup>1</sup>, Zhixin Tai<sup>3,4</sup>, Yajie Liu<sup>3,\*</sup> , Hong Gao<sup>5,\*</sup>   
and Fuqiang Huang<sup>1,6,7,\*</sup>

- <sup>1</sup> State Key Laboratory of High Performance Ceramics and Superfine Microstructure, Shanghai Institute of Ceramics, Chinese Academy of Sciences, Shanghai 200050, China; zhaopei@mail.sic.ac.cn (P.Z.); tangyufeng@mail.sic.ac.cn (Y.T.)
  - <sup>2</sup> School of Physical and Mathematical Sciences, Nanyang Technological University, Singapore 637371, Singapore; jun.pan@ntu.edu.sg
  - <sup>3</sup> Center of Advanced Materials and Technology, Jiangmen Laboratory of Carbon Science and Technology, Jiangmen 529020, China; zhangdongqi@hkustgz-jcl.ac.cn (D.Z.); taizhixin@hkustgz-jcl.ac.cn (Z.T.)
  - <sup>4</sup> National United Engineering Laboratory for Biomedical Material Modification, Branden Biomedical Park, Qihe Advanced Science & High Technology Development Zone, Qihe 251100, China
  - <sup>5</sup> Joint International Laboratory on Environmental and Energy Frontier Materials, School of Environmental and Chemical Engineering, Shanghai University, Shanghai 200444, China
  - <sup>6</sup> Center of Materials Science and Optoelectronics Engineering, University of Chinese Academy of Sciences, Beijing 100049, China
  - <sup>7</sup> State Key Laboratory of Rare Earth Materials Chemistry and Applications, College of Chemistry and Molecular Engineering, Peking University, Beijing 100871, China
- \* Correspondence: liuyajie@hkustgz-jcl.ac.cn (Y.L.); hgao1122@shu.edu.cn (H.G.); huangfq@mail.sic.ac.cn (F.H.)

**Abstract:** Anodes equipped with limited lithium offer a way to deal with the increasing market requirement for high-energy-density rechargeable batteries and inadequate global lithium reserves. Anode-free lithium-ion batteries (AFLBs) with zero excess metal could provide high gravimetric energy density and high volumetric energy density. Moreover, the elimination of lithium with a bare current collector on the anode side can reduce metal consumption, simplify the cell technological procedure, and improve manufacturing safety. However, some great challenges, such as insufficient cycling stability, significant lithium dendrite growth, as well as unstable solid electrolyte interface, impede the commercial application of AFLBs. Fortunately, significant progress has been made for AFLBs with enhanced electrode stability and improved cycling performance. This review highlights research on the design of anode-free lithium-ion batteries over the past two decades, presents an overview of the main advantages and limitations of these designs, and provides improvement strategies including the modification of the current collectors, improvement of the liquid electrolytes, and optimization of the cycling protocols. Prospects are also given to broaden the understanding of the electrochemical process, and it is expected that the further development of these designs can be accelerated in both scientific research and practical applications.

**Keywords:** anode-free; rechargeable lithium-ion batteries; current collectors; electrolyte; protocols



**Citation:** Zhao, P.; Pan, J.; Zhang, D.; Tang, Y.; Tai, Z.; Liu, Y.; Gao, H.; Huang, F. Designs of Anode-Free Lithium-Ion Batteries. *Batteries* **2023**, *9*, 381. <https://doi.org/10.3390/batteries9070381>

Academic Editor: Changshin Jo

Received: 7 June 2023

Revised: 20 June 2023

Accepted: 30 June 2023

Published: 17 July 2023



**Copyright:** © 2023 by the authors. Licensee MDPI, Basel, Switzerland. This article is an open access article distributed under the terms and conditions of the Creative Commons Attribution (CC BY) license (<https://creativecommons.org/licenses/by/4.0/>).

## 1. Introduction

Rechargeable lithium-ion batteries with high energy density, a long cycling life, a low cost, and a high level of safety are highly desirable for a wide range of applications, from miniaturized electronics to grid energy storage [1–3]. On account of its high theoretical capacity and low redox potential, lithium (Li) metal is regarded as a promising anode for achieving high-energy density batteries [4]. For a long time, lithium metal battery (LMB) reports often depended on impractical cell designs to exaggerate the lifespan of LMBs [5]. In labs, the use of low mass-loading cathodes, excess electrolytes, and thick Li metal as counter electrodes are the most common treatments for achieving a reasonable lifetime and high Coulombic efficiency [6]. Meanwhile, in practical cell applications, it is required to increase the loading of active material, decrease the amount of electrolyte,

and reduce the thickness of the Li foil to maximize the energy density but minimize the cost. Among these, making the lithium foil thinner is the main way to decrease the cost of practical development. The price of making ultra-thin lithium metal is quite high, and the manufacturing techniques used are very complicated due to the high reactivity and viscosity of lithium metal, which further increases the costs [7]. Moreover, the severe safety problems, limited global Li reserves, and challenges associated with the extraction of Li have forced the development of anode-free batteries.

In an anode-free lithium-ion battery (AFLB), the Li metal is plated on the current collector in situ during the first charge process, with the Li source entirely springing from the cathodes. Then, the Li ions can be stripped from the previously formed Li anode and intercalated back to the cathodes during the cycling discharge. Based on such a cell configuration, AFLBs possess several merits, including (1) maximized volumetric and gravimetric energy density at the cell level [8]; (2) improved safety, lower cost, and easier assembly, due to the absence of lithium bulks/foils or anode materials consumption and associated issues such as lithium metal extraction, purification, slurry coating, moisture controlling, etc.; (3) a more valuable tool for evaluating electrochemical performance because of the true Li plating/stripping behavior with zero excess lithium to replenish the irreversible loss [5]; (4) less absorption of electrolytes on the current collector side which can reduce electrolyte consumption and further increase the energy density.

Every coin has two sides. Despite the impressive advantages of zero excess lithium, the intrinsic irreversible plating/stripping process of lithium on the heterogeneous current collectors and consumption when reacting with liquid electrolyte lead to rapid lithium inventory loss [9]. Without an extra Li supply, anode-free cells have a much shorter cycle life and lower Coulombic efficiency (CE) than Li-excess cells [10]. Moreover, the as-deposited Li is more inclined to form a mossy and dendritic morphology on foreign substrates compared to the Li metal's thin layers because of its lithiophobic properties and large initial nucleation barriers [11]. The decomposition of electrolytes will accrue on the interface between the as-deposited lithium and electrolyte, facilitating the formation of a solid electrolyte interphase (SEI). The SEI can passivate the interface of Li as well as prevent side reactions since it could impede the transfer of electrons from the lithium anode to the electrolyte [12]. Nevertheless, the stable SEI cannot be maintained because the volume changes during the plating/tripping of lithium inevitably destroy the SEI and result in the continued decomposition of the electrolyte. The Li inventory will be lost, and the capacity will fade during cycling until the SEI is thick enough to prevent the side reaction and the dendritic growth. To date, many strategies have been reported for regulating the quality of deposition and prolonging the cycle lifespan [13,14]; however, comprehensive and instructive reviews are rare [15–18]. In this review, we provide an overview of the designs of anode-free lithium rechargeable batteries with various cathodes and approaches/strategies for enhancing electrochemical performance (Figure 1) and offer an outlook at last for this nascent and promising field.

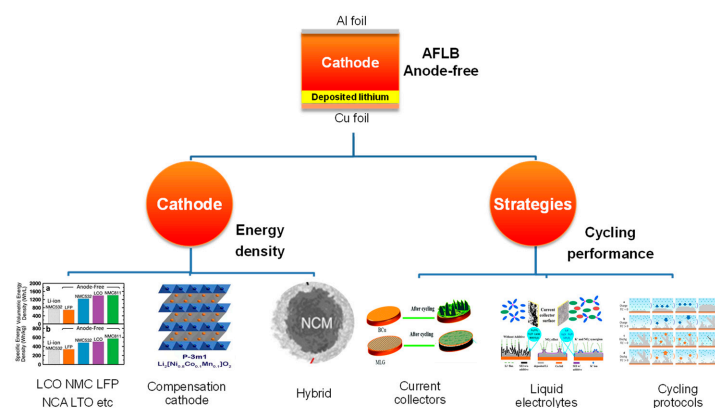


**Figure 1.** Designs of anode-free lithium-ion battery based on cathodes categorization and the strategies for the performance improvement [19–25]. Reprinted with permission from Ref. [20] (Copyright

2021, John Wiley and Sons); Ref. [21] (Copyright 2021, Springer Nature); Ref. [22] (Copyright 2019, RSC Pub); Ref. [23] (Copyright 2019, American Chemical Society); Ref. [24] (Copyright 2019, Elsevier).

## 2. Cathodes of Anode-Free Lithium-ion Batteries

Due to the cathode being the only lithium source in anode-free batteries, the cathodes as a Li reservoir will determine the capacity and energy density of the full cells. The modification of cathodes is considered the most effective way to assemble cells with high energy density; therefore, it is essential to know the delivered energy density based on different cathodes.  $\text{LiCoO}_2$  (LCO),  $\text{LiNi}_x\text{Mn}_y\text{Co}_{1-x-y}\text{O}_2$  (NMC), and  $\text{LiFePO}_4$  (LFP) are the common cathodes in AFLBs. Compared to LCO, NMC delivers a higher capacity and employs less cobalt. According to the ratio of Ni/Mn/Co, there are series of NMC, including  $\text{LiNi}_{0.8}\text{Mn}_{0.1}\text{Co}_{0.1}\text{O}_2$  (NMC811),  $\text{LiNi}_{0.6}\text{Co}_{0.2}\text{Mn}_{0.2}\text{O}_2$  (NMC622),  $\text{LiNi}_{0.5}\text{Mn}_{0.3}\text{Co}_{0.2}\text{O}_2$  (NMC532),  $\text{LiNi}_{1/3}\text{Mn}_{1/3}\text{Co}_{1/3}\text{O}_2$  (NMC111), etc.

Louli et al. tried to figure out how different cathodes with different sources of lithium could impact the reversible plating of lithium by using the four most commonly used positive electrodes: NMC532, NMC811, LCO, and LFP [19]. The authors investigated these cathodes operating in different influence factors, such as upper cut-off voltage, depths of discharge, electrolytes, temperatures, and pressures. NMC811 and LCO anode-free cells exhibited the highest initial volumetric energy density both of  $1400 \text{ Wh L}^{-1}$ , while NMC532, LFP, and NMC532 lithium-ion cells showed lower values of  $1200 \text{ Wh L}^{-1}$ ,  $700 \text{ Wh L}^{-1}$ , and  $700 \text{ Wh L}^{-1}$ , respectively. Furthermore, the cycling behavior showed some differences, despite the similar ultimate lifespan of the batteries. The LCO anode-free cells had a linear energy fade in the first 60 cycles and along with a rapid decay after 60 cycles. The energy density decay of cells with NMC811 was more serious than cells with NMC532, not only in the initial but in the last cycles. The NMC532 cells showed the most stable cycling behavior in the first 50 cycles ahead of more significant energy density decay. The LFP cells exhibited the lowest volumetric energy density among all anode-free chemistries with the most severe energy fade (Figure 2). It should be noticed that this result only reveals the cycling performance under specific conditions using dual-salt electrolytes. NMC811 cells can deliver a relatively high specific capacity and contain less cobalt in components, which is beneficial in cost, output energy density, and humanitarian points of view. LFP cathodes, based on abundant and low-cost iron, with long cycle life are becoming more popular. Similarly, the LCO cathode does exhibit a significant irreversible capacity and it has better rate performance and higher cut-off voltage. Therefore, which cathode should be chosen depending on the real-life demand.

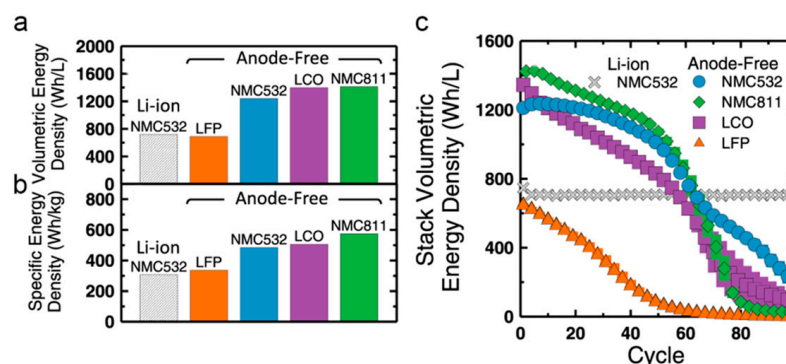


**Figure 2.** Volumetric energy density (a), specific energy density (b), and cycling performance (c) of anode-free lithium-ion cells with LFP, NMC532, LCO, and NMC811 as cathodes compared to a conventional Li-ion cell with an NMC532 as a cathode [19]. Figures from [19] under CC BY 4.0 license, without any changes.

$\text{LiNi}_{0.9}\text{Co}_{0.05}\text{Al}_{0.05}\text{O}_2$  (NCA) [26],  $\text{LiNi}_{0.95}\text{Mn}_{0.015}\text{Co}_{0.02}\text{Al}_{0.01}\text{Mg}_{0.005}\text{O}_2$  (NMCAM) [27],  $\text{Li}_4\text{Ti}_5\text{O}_{12}$  (LTO) [28],  $\text{Li}_2\text{S}$  [29–32], and lithium compensation cathodes (pre-lithiated  $\text{TiS}_2$  [33], Li-rich compounds like  $\text{Li}_2[\text{Ni}_{0.8}\text{Mn}_{0.1}\text{Co}_{0.1}]\text{O}_2$  ( $\text{Li}_2\text{NMC811}$ ) [20],  $\text{Li}_2\text{Ni}_{0.5}\text{Mn}_{1.5}\text{O}_4$

( $\text{Li}_2\text{NMO}$ ) [34], and self-sacrificing materials [35]) were also investigated in AFLBs. Besides the single-component cathode materials, there are hybrid ones developed to enhance the reversible capacity. Four hybrid cathodes with different ratios of NMC811 and  $\text{Li}_2\text{CuO}_2$  were expressed as  $(80-x)\text{NMC}-x\text{Li}_2\text{CuO}_2$ , and the mass loading of all electrodes was around  $5.0\text{--}5.5\text{ mg cm}^{-2}$  [36]. The reversible capacity and the cycling stability were remarkably enhanced as the increase in the  $x$ . The capacity faded very fast for the cell with  $x = 0$ , and the capacity linearly declined to zero only after nearly 40 cycles. With the increase of  $\text{Li}_2\text{CuO}_2$ , the cycling stability of cells was dramatically improved. As the value of  $x$  increased to 40, the cell can maintain more than 70% capacity retention (CR) after 140 cycles at  $0.5\text{ mA cm}^{-2}$  (Figure 3a). With the higher  $\text{Li}_2\text{CuO}_2$ , the cell's performance is improved, which is likely associated with the integrity of the Li primer layer. When the  $x$  is low, the amount of Li deposits may not be sufficient to fully cover the surface of the current collector. As  $x$  increases, a more uniform and complete layer can be formed so that the cell could have better cyclability. The requirement for the thickness of the practical Li layer is almost the same for various cathodes. Hence, minimizing the weight percentage of  $\text{Li}_2\text{CuO}_2$  and augmenting the loading of the composite cathode could compensate for the energy density loss resulting from the additional weight of  $\text{Li}_2\text{CuO}_2$ , which design of the battery could maintain a high energy density.

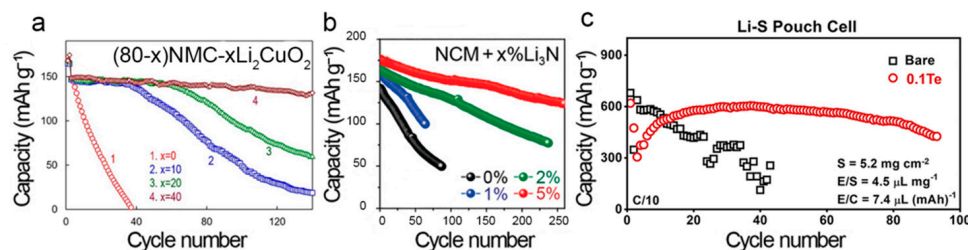


**Figure 3.** Electrochemical performance of the anode-free cells with hybrid cathodes: (a) NMC811 +  $\text{Li}_2\text{CuO}_2$ , (b) NMC622 +  $\text{Li}_3\text{N}$  (c) S + Te. Reprinted with permission from Ref. [32] Copyright 2020, Elsevier; [36] Copyright 2018, Elsevier; [37] Copyright 2021, John Wiley and Sons.

Motivated by the designs of anion donors in anode-free architecture,  $\text{Li}_2\text{O}$  (as an additional Li source) was preloaded to the NMC811 to compensate for the irreversible Li consumption during charge/discharge [21]. It can provide  $\sim 1.75$ -fold excess Li in the decomposition of the  $\text{Li}_2\text{O}$  component compared to the active Li reserved within the NMC811.  $\text{Li}_2\text{O}$  preloaded on the NMC811 not only acts as a Li donor, providing an additional Li source to offset the irreversible loss of Li but also acts as a bifunctional sacrificial agent which can produce  $\text{Li}^+$  and  $\text{O}^{2-}$  contributing to the construction and stabilization of the cell architecture. Specifically, the produced  $\text{O}^{2-}$  from  $\text{Li}_2\text{O}$  can react with electrolyte additives to in situ form the LiF-based passivation layer for the cathode, which could stabilize the electrode and further improve the cyclability of cells. Based on this composite cathode design, the coin cell presented a high CR of 90% after 300 cycles, while the pouch cell demonstrated a high energy density beyond  $320\text{ Wh kg}^{-1}$  and delivered reversible 300 cycles with a CR of 80%.

A sacrificial lithium nitride ( $\text{Li}_3\text{N}$ ) was also introduced in the NMC622 in order to boost cycling stability [37]. To assess the effect of  $\text{Li}_3\text{N}$  percentage (ranging from 0% to 5%) on cell performance, pressurized cells were fabricated with a high-Ni NMC as cathode and indium (free lithium) as a counter/reference electrode. Along with the increase in  $\text{Li}_3\text{N}$ , the delivered charge/discharge capacity increased due to the decomposition of the  $\text{Li}_3\text{N}$  which not only provided supplementary Li to compensate for the consumed Li via side reaction but also increased the internal cell pressure to keep good physical contact among the components during cycling. Moreover, the CR for the cell with 0%  $\text{Li}_3\text{N}$  was 37.9% after 80 cycles, whereas it showed an excellent CR of 75.8% over 200 cycles with additive  $\text{Li}_3\text{N}$  of 5% in the composite cathode (Figure 3b).

Introducing an additive of elemental tellurium ( $\text{Te}^0$ ) in the sulfur or  $\text{Li}_2\text{S}$  cathode could lead to a great improvement in the reversibility and cyclability of the anode-free full cells [32]. During cycling,  $\text{Te}^0$  tends to react with the generated polysulfides ( $\text{Li}_2\text{S}_n$ ) to produce polytellurosulfide ( $\text{Li}_2\text{Te}_x\text{S}_y$ ) species. The soluble  $\text{Li}_2\text{Te}_x\text{S}_y$  can migrate to the anode and further decompose on the deposited Li surface to form a novel SEI layer, which consists of the components of  $\text{Li}_2\text{TeS}_3$  and  $\text{Li}_2\text{Te}$ . The Te-contained SEI conferred a huge contribution to stabilizing Li deposition. The as-prepared pouch cell with Te additives could maintain long cycling stability for more than 100 cycles, while the counterparts of pouch cells without Te additives could only maintain 14% capacity retention after 40 charge/discharge cycles (Figure 3c). It should be noticed that the additives without lithium could cut down the advantage of anode-free design in terms of energy density.

### 3. Strategies Applied to AFLB and Improvement

The main strategies for enhancing the performance of full cells, including modification of the current collectors, improvement of the liquid electrolytes, and optimization of the cycling protocols. As for each strategy, we classify the groups according to the cathode type.

#### 3.1. Modification of the Current Collectors

Copper (Cu) foil is commonly used as a current collector in AFLB because Cu cannot be intercalated by Li. The irreversible plating/stripping of Li on the current collector of Cu and a more serious dendrite growth on Cu than on thin Li metal inspires us to improve/modify the current collector because the current collector can play a crucial role in the Li nucleation and growth of deposited Li, which significantly affects the Coulombic efficiency and cycling performance of the AFLB. Yi Cui's group elucidated the relationship between lithium nuclei shape, size, areal density, and current rate, consistent with the classical crystalline grain nucleation and growth theory [38]. The discovered fundamental scientific theory could provide a guideline for the modification of current collectors.

A variety of approaches have been proposed by worldwide researchers, including layer coating modification of the current collector, three-dimensional (3D) design of the current collector, surface modification, and the development of alternative current collectors instead of Cu.

Modifying the current collector by layer coating is reported in most research work, which can effectively decrease the initial nucleation barrier, facilitate the uniform deposition of Li, and enhance the electrochemical properties with long cycling stability. However, based on this layer coating design, the extra weight and volume have to be taken into consideration to maintain the advantage of energy density in the anode-free battery. Moreover, it is worth to be mentioned that the physicochemical property of the coating layer should be identified, which always be ignored in previous published studies. If the coating layer is only ionic conductive, it can be regarded as a solid electrolyte; if it is both ionic and electric conductive, it can be deemed as an anode and the cell cannot be strictly called the anode-free cell; only when it is electric conductive, it can be seen as a current collector coating layer. These sorts listed above are very simple models and easy to separate, while the practical cases are more complicated. Besides the electric conductive of inert layers, some other properties of the coating layer such as adhesion, stability, and uniformity should also be considered.

The 3D structured design of the current collector could accommodate the volume change of Li during Li deposition, reduce the local current density, and further suppress the dendrite growth with prolonged cycle life. Nevertheless, the intrinsic low lithiophilicity of Cu current collectors inevitably causes a high nucleation barrier, which can hardly achieve homogeneity of deposited Li. So, the 3D structured current collector always along with surface modification with kinds of nucleation seeds to decrease the nucleation barrier. [39]. Surface modification by heat treatment of Cu current can also improve the anode interphase and lead to enhanced lithiophilicity of Cu foil and homogeneous Li deposition [40].

By replacing the current collector of Cu with other current collectors, it can enhance the binding energy with lithium and lower the nucleation barrier of Li to promote the cyclability of cells. Alternative current collectors like stainless steel (SS) [26,37,41], bare nickel (Ni) foil [32], and gold sputter perforated polyimide film (PI@Au) [42] substrates also served as anode current collectors in AFLBs to improve electrochemical performance. Furthermore, alternative current collectors with lower density than Cu might achieve high energy density batteries. Nevertheless, sometimes, we need to balance the resulting performance with manufacture cost based on the alternative current collector instead of Cu.

The above-mentioned various approaches for modifying the current collector could be presented in detail in different cathodes system as follows.

### 3.1.1. NMC Cathode

Bing Joe Hwang's group explored different coating layers on copper current collectors using NMC111 as a cathode.

Li ion conductive film, consisting of cubic garnet of  $\text{Li}_7\text{La}_{2.75}\text{Ca}_{0.25}\text{Zr}_{1.75}\text{Nb}_{0.25}\text{O}_{12}$ , lithium perchlorate ( $\text{LiClO}_4$ ) salt and polyvinylidene fluoride (PVDF), was prepared via electrospinning preparation. The anode-free full cell configuration demonstrated an improved CR of 58.66% after 30 cycles with an average CE of 97.6% (Figure 4a) [43].

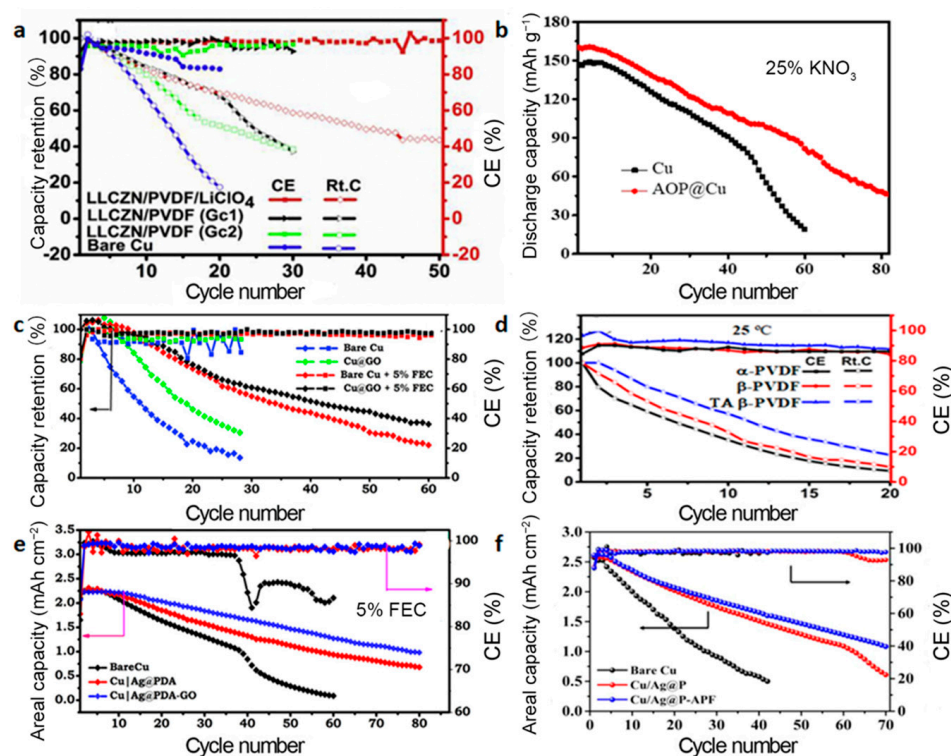


**Figure 4.** Comparison of the CR and CE versus cycle number using NMC111 cathodes and various coating layers (a–f) on copper current collectors under  $0.2 \text{ mA cm}^{-2}$  except (e) at  $0.5 \text{ mA cm}^{-2}$ . Reprinted with permission from Ref. [43] Copyright 2018 Elsevier, Ref. [44] Copyright 2020 American Chemical Society, Ref. [45] Copyright 2020 Elsevier, Ref. [46] Copyright 2021 American Chemical Society, Ref. [47] Copyright 2021 Elsevier, Ref. [48] Copyright 2021 Elsevier.

Cu covered with a grounded  $\text{Al}_2\text{O}_3$ /polyacrylonitrile composite layer (AOP) as AOP@Cu was reported to promote the compact and smooth lithium deposition. The as-prepared anode-free full cell exhibited enhanced cycling stability and CE. It exhibited discharge capacity of  $160 \text{ mAh g}^{-1}$  in the first cycle and retained 30% of capacity after 82 cycles, whereas the Cu|NMC111 full cell retained  $\sim 30\%$  only after 52 cycles (Figure 4b) [44].

An ultra-thin spin-coated binder-free graphene oxide (GO) was used to modify the Cu current collector. The AFLB with GO film was able to achieve a high CE of 98% and

attained ~44% of its initial capacity after 50 cycles. While the full cell with bare Cu had a CE of 89% and retained 26.9% after 20 cycles (Figure 4c) [45].

A conformal coating of  $\beta$ -PVDF polymer on copper was prepared by electrospinning. When the Cu@ $\beta$ -PVDF||NMC111 cell was treated at 60 °C with the first five charge/discharge cycles, termed thermal-electrochemical activation (TEA), it achieved a CR of 68.36% at the 20th cycle (Figure 4d) [46].

Cu was coated by lithiophilic silver nanoparticles with polydopamine (Ag@PDA) layer. This layer can be used as a nucleation seed. Then, graphene oxide (GO) was coated on Ag@PDA to act as an artificial SEI to buffer the Li-ion distribution in AFLBs. This anode-free full cell with modified copper as anode and NMC111 as cathode showed a high average CE of ~98.6% and high CR of ~55.7% after 60 cycles in the carbonate-based electrolyte with 5% FEC at 0.5 mA cm<sup>-2</sup>. However, the bare Cu collector with no coating only achieved the average CE and CR of 94.4% and 4.3%, respectively (Figure 4e) [47].

A two-step modification with Ag@PDA and an artificial protection film (APF) on the copper surface was designed as interfacial functional double layers. Poly (vinylidene fluoride-cohexafluoropropylene) to LiTFSI in 5:2 is the component of APF. With modified copper, the anode-free cell exhibited a superior CE of 98.15%, and maintained 40% CR over 70 cycles compared to the CE of 96.18% and 40% CR after 25 cycles for the cells without Cu modification under the current density of 0.2 mA cm<sup>-2</sup> (Figure 4f) [48].

Marnix Wagemaker's group exploited the cycling efficiency of the anode-free coin cells with a BaTiO<sub>3</sub>-coated Cu electrode and a NMC811-based positive electrode. The full cell presented an average CE of 99.37% and a CR of 75% over 70 cycles [49].

With liquid metal (LM) coating layer, an epitaxy-induced electro-plating Cu (E-Cu) and NMC811 cathode were also used in AFLBs. The LM consists of Ga, In, and Sn (mass ratio of 68.5:21.5:10). By alloying reaction to form an epitaxial-induced layer, the functional LM layer can initiate Li storage. The anode-free pouch cell was assembled with lean electrolyte addition of 2 g Ah<sup>-1</sup> and high mass loading of 25 mg cm<sup>-2</sup>. After more than 50 cycles, the CR increased from 66% to 84%. The remarkable energy density reached 420 Wh kg<sup>-1</sup> by using E-Cu instead of a normal Cu current collector [50].

### 3.1.2. LFP Cathode

Bing Joe Hwang's group used a Cu current collector covered with polyethylene oxide (PEO) films to reveal the uniform deposition of Li and suppression of dendrite. They tested the AFLB experimentally by integrating the coated copper with an LFP cathode into a full cell. The cell exhibited good cycling performance with an average CE of 98.6% and CR of 30% after 200 cycles (at 0.2C) (Figure 5a) [51].

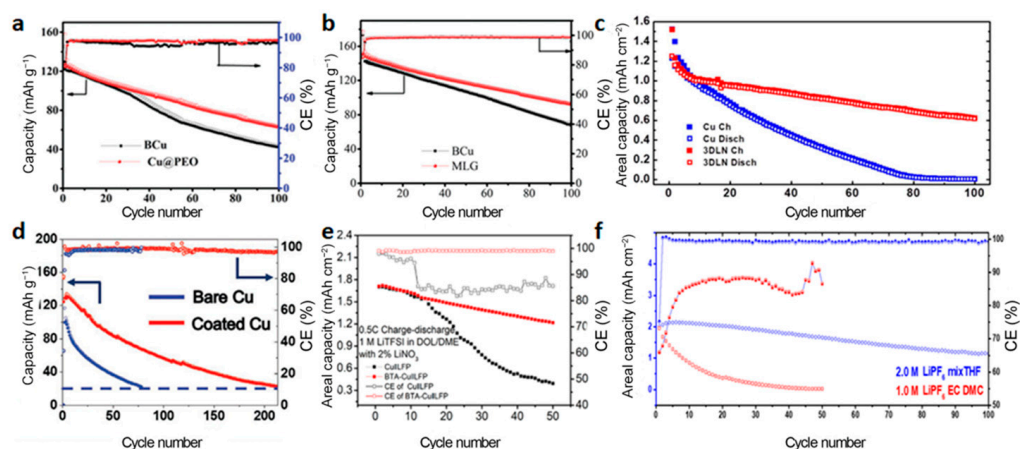


**Figure 5.** Comparison of CR and CE versus cycle number using LFP cathodes and various coating layers on copper current collectors (a–f). Reprinted with permission from Ref. [22] Copyright 2019

Royal Society of Chemistry. Ref. [51] Copyright 2018 RSC hub, Ref [52] Copyright 2019 Elsevier, Ref. [53] Copyright 2020 John Wiley and Sons, Ref. [54] Copyright 2020 American Chemical Society, and Ref. [55] Copyright 2020 Elsevier.

Using thin-film  $\text{Cu}_3\text{N}$ -modified copper foil as an anode current collector and LFP as a cathode, the full-cell exhibited enhanced cycling stability and low overpotential. A multifaceted study demonstrated that after initial lithium plating,  $\text{Cu}_3\text{N}$  can be converted to a  $\text{Li}_3\text{N}/\text{Cu}$  nanocomposite, and form a highly uniform conductive network in situ [56].

With ultrathin multilayer graphene (MLG) growing on a Cu current collector via chemical vapor deposition (CVD), it can be used to stabilize the electrode interface as an artificial layer. Paired with a commercial LFP cathode with mass loading of  $\sim 12 \text{ mg cm}^{-2}$ , this full cell delivered the initial discharge capacities of  $147 \text{ mA h g}^{-1}$  for bare electrodes and  $151 \text{ mA h g}^{-1}$  for multilayer-graphene-protected electrodes, respectively. After 100 cycles, the bare Cu and multilayer graphene-protected electrodes maintained  $\sim 46$  and  $\sim 61\%$  of the initial capacities, respectively at the rate of  $0.1 \text{ C}$  (Figure 5b) [22].

A scalable 3D electrode fabricated by coating the well-mixed  $\text{LiNO}_3$ , carbon black, and PVDF slurry on the Cu current collector and the fabricated AFLB cells exhibited a good CR of  $49.1\%$  after 100 cycles with an average efficiency of  $99.3\%$  (Figure 5c) [52].

Derived from a commercial adhesive tape, the use of a laser-induced silicon oxide ( $\text{Li-SiO}_x$ ) layer for current collector modification was studied. The capacity retention was  $45.6\%$  after 100 cycles with an average CE of  $99.2\%$ . As the areal capacity increased from  $0.9$  to  $2.6 \text{ mA h cm}^{-2}$ , the capacity retention can reach  $52.8\%$  after 100 cycles. Cells with bare Cu only remained  $21.8\%$  of original capacity and the average CE was  $98.1\%$  (Figure 5d) [53].

Benzotriazole (BTA) can modify the Cu foil surface and induce homogeneous Li plating because of the lithiophilic property of the N atom in the BTA molecule. The anode-free architecture of BTA-Cu || LFP exhibited a  $\sim 73.3\%$  CR of the initial capacity at the 50th cycle (Figure 5e) [54].

A uniform Li nucleation can be led by a lithiophilic bismuth graphite (Bi-Gr) substrate with a lithiophobic LiF-rich SEI. The molecular dynamic simulation showed that, in a  $2.0 \text{ M LiPF}_6$  in tetrahydrofuran/2-methyl tetrahydrofuran ( $2.0 \text{ M LiPF}_6\text{-mixTHF}$ ) electrolyte, the preferential reduction of anions can generate a LiF-rich SEI on the surface of deposited Li. Bi-Gr substrate and electrolyte enabled the anode-free LFP full cells to achieve 100 cycles at an areal capacity of  $>2.0 \text{ mA h cm}^{-2}$  (Figure 5f) [55].

An anode-free full cell configuration coupled with LFP cathodes also demonstrated that the electrochemical performance can be enhanced by coating LiF@PVDF on Cu foil even under the harsh condition of limited lithium sources in AFLB [57].

### 3.1.3. Other Cathodes

A Li-free solid-state battery was introduced with  $\text{LiCoO}_2$  as a cathode and Lipon as an electrolyte. The cycling stability with only a copper current collector was poor, and almost half of the reversible capacity was lost during the initial cycles. Two different overlayers on Cu, glassy Lipon, and plastic parylene were compared for cycling over 1000 times between  $4.2$  and  $3.0 \text{ V}$  at  $1 \text{ mA/cm}^2$ . The battery with the parylene overlayer showed only a capacity fade of  $20\%$  over 1000 cycles, whereas the cell with the Lipon overlayer showed a  $26\%$  capacity loss (Figure 6a,b) [58].

By pre-plating a thin tin layer on the existing Cu foil, a Li-Sn alloy can be formed by the reaction between Li and the Sn metal, and then Li metal can deposit on the surface of Li-Sn alloy instead of Cu substrate. The Cu ||  $\text{LiNi}_{0.85}\text{Co}_{0.10}\text{Al}_{0.05}\text{O}_2$  (NCA) cell can maintain reversible cycling for about 30 cycles, and the Sn-Cu || NCA cell can achieve 80 cycles before a severe capacity decline (Figure 6c) [59].

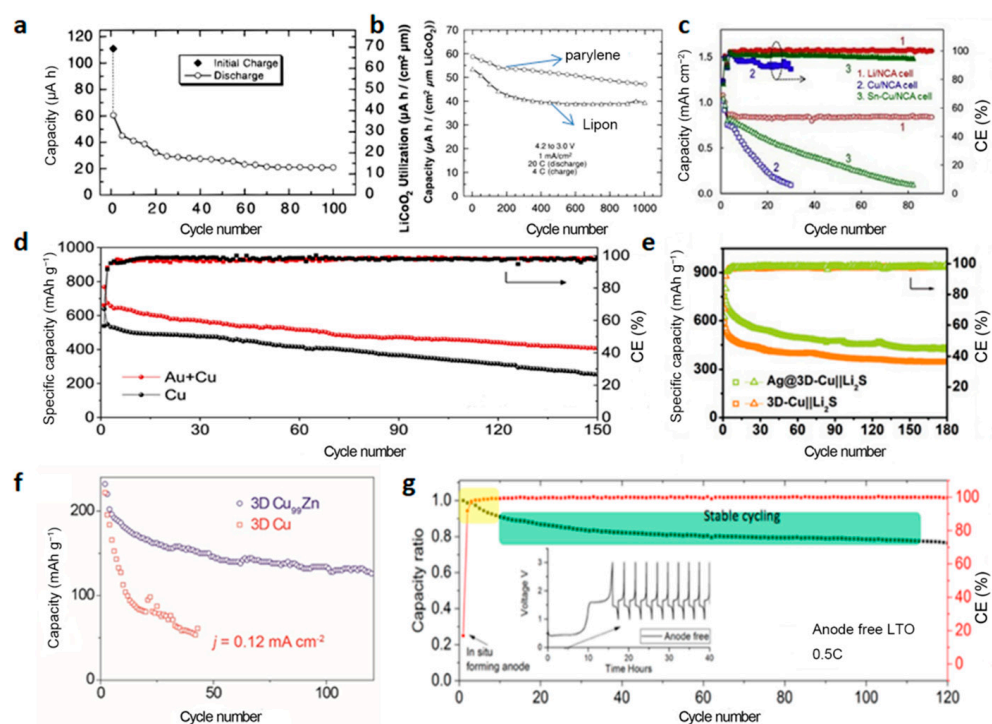


**Figure 6.** Comparison of CR and CE versus cycle number using (a,b) LiCoO<sub>2</sub>, (c) NCA (d,e) Li<sub>2</sub>S (f) pre-lithiated TiS<sub>2</sub> and (g) LTO cathodes and various coating layers on copper current collectors. Reprinted with permission from Ref. [28] Copyright 2018 American Chemical Society, Ref. [29] Copyright 2021 Royal Society of Chemistry, Ref. [31] Copyright 2020 Elsevier, Ref. [33] Copyright 2018 Elsevier, Ref. [58] Copyright 2000 IOP Publishing and Ref. [59] Copyright 2017 Elsevier.

With Au-modified Cu foil as “anode” and Li<sub>2</sub>S as cathode, an anode-free full cell can achieve a high energy density (up to 626 Wh kg<sup>-1</sup>). The Au modification can be transformed to Li<sub>x</sub>Au alloy, which could decrease the Li nucleation barrier and obtain the Li deposition layer with thick and dendrite-free morphology. The Au/Cu || Li<sub>2</sub>S cell delivered first discharge capacity of 770 mA h g<sup>-1</sup> with an initial CE of 69.5%, while as for the Li<sub>2</sub>S || Cu chemistry, the first discharge capacity was 639 mA h g<sup>-1</sup> with the initial CE of 56.6%. The Li<sub>2</sub>S || Au/Cu cell maintained a discharge capacity of 409 mA h g<sup>-1</sup> with a CR of 53%, whereas the Li<sub>2</sub>S || Cu cell only maintains 254 mA h g<sup>-1</sup> with a CR of 40% after 150 cycles (Figure 6d) [31].

The Ag@3D-Cu || Li<sub>2</sub>S batteries with a Li<sub>2</sub>S loading of 3.8 mg cm<sup>-2</sup> demonstrated a greater initial discharge capacity (752.4 mA h g<sup>-1</sup>) compared to that of the 3D-Cu || Li<sub>2</sub>S battery (588.4 mA h g<sup>-1</sup>). The reversible capacity of Ag@3D-Cu || Li<sub>2</sub>S battery was 424.1 mA h g<sup>-1</sup> after 180 cycles, while the capacity of 3D-Cu || Li<sub>2</sub>S battery was merely 349.2 mA h g<sup>-1</sup>. Moreover, the initial CE of the Ag@3D-Cu || Li<sub>2</sub>S battery was 70.7%, which is higher than that of the 3D-Cu || Li<sub>2</sub>S battery (65.3%). (Figure 6e) [29].

The modification of the commercial Cu current collector with atomically distributed Zn artificial defects was obtained via magnetic sputtering of Cu<sub>99</sub>Zn. The prepared current collector was assembled into anode-free full cells with pre-lithiated TiS<sub>2</sub> cathodes. The batteries with 3D Cu<sub>99</sub>Zn electrodes showed better cycling performance compared to that with pure Cu electrodes (Figure 6f) [33].

By incorporating a new, high-efficiency electrode design, cells with 15 nm thick Al<sub>2</sub>O<sub>3</sub>-Cu || LTO cells were reported. It yielded stable and efficient lithium plating/stripping at a current density of 3 mA cm<sup>-2</sup> with a CE > 98% over 120 cycles (Figure 6g) [28].

### 3.2. Improvement of the Liquid Electrolytes

Electrolyte has played an indispensable role in cycling stability of lithium-ion batteries. All of the choices such as electrolyte salt species and solvent types, electrolyte concentra-

tions, and electrolyte additives can affect the solvation of electrolytes and, therefore, modify the in situ formed SEI. Meanwhile, liquid electrolyte modification has a minor impact on the whole energy density of cells as the increased weight can be negligible. The commercial and basic electrolyte solvents can be divided into carbonate-based and ether-based solvents.

Some carbonate-based solvents in the following examples are listed here: diethyl carbonate (DEC), dimethyl carbonate (DMC), ethylene carbonate (EC), ethyl methyl carbonate (EMC), fluoroethylene carbonate (FEC), 3,3,3-fluoroethylmethyl carbonate (FEMC), propylene carbonate (PC) and vinylene carbonate (VC). And ether-based solvents are also listed: diethylene glycol dimethyl ether (DGDE), 1,2-dimethoxyethane (DME), 1,3-dioxolane (DOL), 1,1,2,2-tetrafluoroethyl-2',2', 2'-trifluoroethyl ether (HFE), 1,1,2,2-tetrafluoroethyl-2,2,3,3-tetrafluoropropyl ether (TTE), etc.

Electrolyte salts commonly used are lithium hexafluorophosphate ( $\text{LiPF}_6$ ), lithium tetrafluoroborate ( $\text{LiBF}_4$ ), lithium bis(trifluoromethanesulfonyl)imide ( $\text{LiTFSI}$ ), lithium bis(fluorosulfonyl)imide ( $\text{LiFSI}$ ), lithium difluoro(oxalate)borate ( $\text{LiDFOB}$ ), lithium trifluoromethanesulfonate ( $\text{LiCF}_3\text{SO}_3$ ), etc.

Replacing the liquid electrolyte with the solid-state electrolyte (SSE) does not change the volumetric energy density considering the SSE has the same volume as the electrolyte and separator in the liquid cell. However, it reduces the gravimetric energy density because of the higher density of SSE than liquid. Even though, the energy density is still comparable to the ones of the lithium metal battery. Excellent cycle lifespan (>1000 cycles) that far exceeds any reported work on anode-free cells is obtained in anode-free solid batteries with Lipon/ $\text{Li}_6\text{PS}_5\text{Cl}$  as electrolytes [26,58]. The key challenges are the low ionic conductivity of electrolytes and high interfacial transfer resistance between the cathode and electrolyte. The current developments, issues, and challenges in anode-free solid-state batteries have been comprehensively reviewed [8,60]. Here, in this part, we focus on the development of liquid electrolytes and their modifications along with performance effects exhibited in different cathode systems as follows.

### 3.2.1. NMC Cathode

After Li deposited on Cu current collector during the first discharge in the  $\text{Cu} \parallel \text{NMC111}$  cell with 1.2 M  $\text{LiPF}_6$  in EC:EMC (30:70 wt%) as electrolyte, the following discharge capacity only recovered 23% of the first charge capacity of the full cell (Figure 7a) [9].

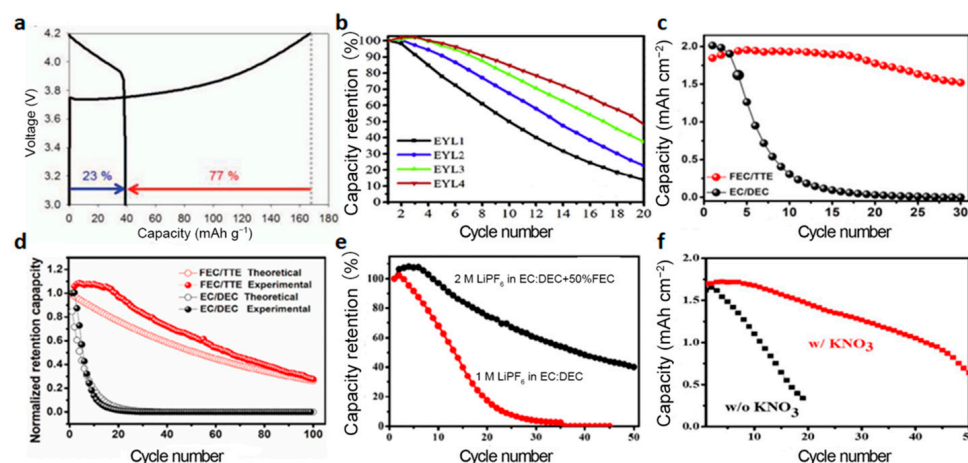


**Figure 7.** Comparison of CR and CE versus cycle number using NMC111 cathodes and various electrolyte additives (a–f). Reprinted with permission from Ref. [9] Copyright 2014 IOP Publishing, Ref. [23] Copyright 2019 American Chemical Society, Ref. [24] Copyright 2019 Elsevier, Ref. [61] Copyright 2019 Elsevier, Ref. [62] Copyright 2020 Elsevier.

Bing-Joe Hwang's group reported that dual additives for electrolytes in full cell configuration of  $\text{Cu} \parallel \text{NMC111}$  can dramatically improve the average Coulombic efficiency, cycling performance, and capacity retention of the cell. It was reported that the CR of

48% can be retained at the 20th cycle for anode-free cells with 2 wt% KPF<sub>6</sub>-2 vol% TMSP additives in the electrolyte, while the CR of 14% only was reached for the counterpart cell with commercial electrolyte without any additives (Figure 7b) [61].

Development of electrolyte additives could be an effective way to promote the non-flammable and high-voltage electrolyte. Based on the anode-free cell of Cu||NMC111, two extreme electrolytes were compared to understand the fundamental science behind them. The cells with the electrolyte of LiPF<sub>6</sub> in a mixture solvents of FEC and TTE showed super cycling stability, retaining 85% of its initial capacity after 30 cycles' charge/discharge with an average CE of ~98% at 0.5 mA cm<sup>-2</sup> (Figure 7c,d) [62].

AFLB of Cu||NMC111 with a locally concentrated electrolyte (2 M LiPF<sub>6</sub> in EC/DEC with FEC) showed great cycling stability with an average CE of 97.8% and a CR of 40% after 50 cycles. However, the common carbonate-based electrolyte had an average CE below 90% and a CR below 40% even in the 15 cycles (Figure 7e) [23].

The Cu||NMC111 cell possessed a CR of ~40% at the 50th cycle in the existence of KNO<sub>3</sub> additive in the electrolyte, while compared to the same value of CR, it only can maintain 15 cycles in the counterpart electrolyte, 1 M LiPF<sub>6</sub> in EC/DEC. The average CE of Cu||NMC111 cell with electrolyte additive was 96.50% after 50 cycles, whereas it was 91.32% after 35 cycles without KNO<sub>3</sub> (Figure 7f) [24].

J. R. Dahn et al. discussed the cycling behavior of pouch cells of NMC532||Cu under an ultra-high-precision-charger (UHPC) process, in which the cells can be operated under low or high pressure in two kinds of electrolytes (1.0 M LiPF<sub>6</sub> FEC:TFEC 1:2, *v/v*; 1.0 M LiPF<sub>6</sub> FEC:DEC 1:2, *v/v*). The performance parameter of CR and CE can be significantly affected when the lower cutoff voltage was decreased from 3.6 V to 1.25V (Figure 8a). As the lower cutoff voltage decreased to 1.25 V, it showed a linear capacity fade with a poor constant CE < 99% and an improved output capacity after 60 cycles. Moreover, relatively accurate predictions of the cells' lifetime (FEC:TFEC > FEC:DEC; high pressures > low pressure) had been made based on the measurements of CE after the deep discharge for 5–10 cycles [63].

They evaluated the cycling performance of AFLB pouch cells (NMC532||Cu) with operando pressure measurements (75–2205 kPa) in different electrolytes. It was reported that the initial average pressure in a certain range (75–1200 kPa) could prolong the cycle life of cells both in FEC:TFEC and FEC:DEC electrolytes (Figure 8b). They also discovered that the effect of high pressure (in the range of 1200 to 2200 kPa) on the cycling performance of AFLB in different electrolyte systems was inconsistent, suggesting in the high-pressure range the physical characteristics of electrolyte lead a key role in the cells' performance instead of the pressure influence factor [64].

The anode-free pouch cell of Cu||NMC532 could deliver a high CR of 80% after 90 cycles when it was equipped with a dual salt LiDFOB/LiBF<sub>4</sub> electrolyte (Figure 8c) [65].

The cells with the high-concentration dual-salt (2.0 M LiDFOB and 1.4 M LiBF<sub>4</sub> mixture) electrolyte in Cu||NMC532 outperformed the cells with 0.6 M LiDFOB and 0.6 M LiBF<sub>4</sub> mixture salts in electrolytes, sustaining a lifetime of more than 200 cycles under high pressure at 20 °C (Figure 8d) [66].

The Cu||NMC532 cells with 1.0 M lithium difluoro (oxalate) borate (LiDFOB) and 0.05 M lithium hexafluorophosphate in FEC/TTE/DEC electrolyte (2:2:1 *v/v/v* ratio) can output superior electrochemical properties than the cells with FEC/TTE electrolyte (2:3 *v/v* ratio). A capacity retention of 45% was obtained for the FEC/TTE/DEC electrolyte, while a CR of only 8% was achieved for FEC/TTE electrolyte (Figure 8e) [67].

Anode-free cells with NMC622 as cathode were used to test the electrolytes. The capacity of the cells with Gen II as an electrolyte can decay significantly to barely zero after 30 cycles. Meanwhile, the cells with BSEE (4.6 m LiFSI + 2.3 m LiTFSI-DME) surpassed the cells with SSEE (4.6 m LiFSI-DME), with initial CEs of 80.5% vs. 78.1%, and a residual capacity of 90.9 mA h g<sup>-1</sup> and CE of 98.6% as compared to 54.8 mA h g<sup>-1</sup> and a CE of 97.4% for SSEE (Figure 8f) [68].

The non-flammable electrolyte comprised of 1 M LiPF<sub>6</sub> in a mixture solvent of FEC: FECM: HFE, 2:6:2 by weight, was introduced. This all-fluorinated electrolyte made the cells of Cu || NMC811 deliver a 60 times higher capacity than that of cells with EC/DMC electrolyte (Figure 8g) [69].

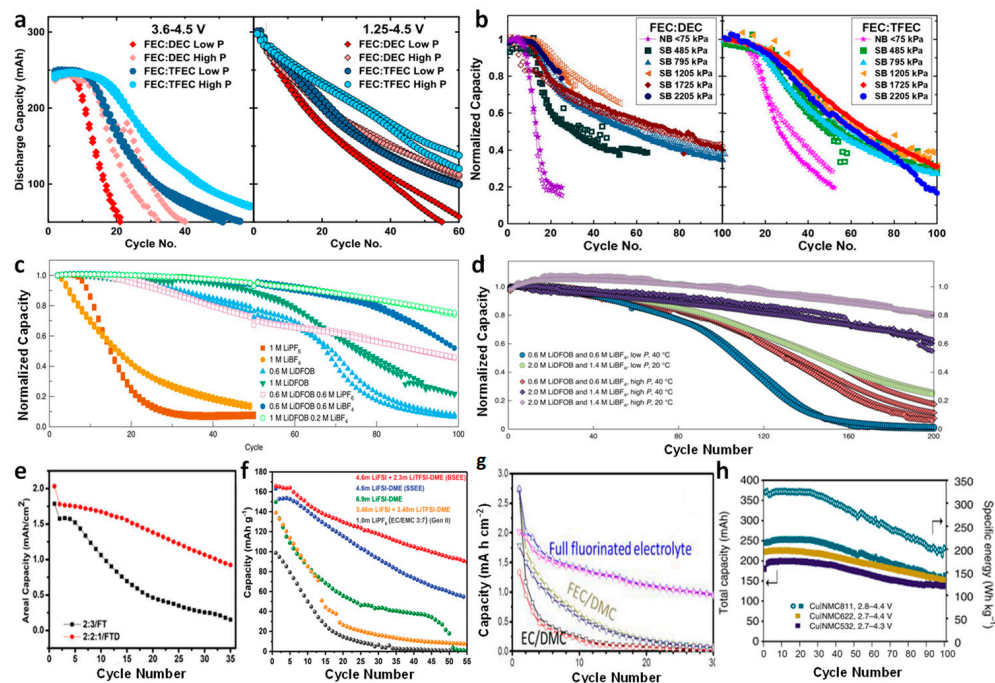


**Figure 8.** Comparison of CR and CE versus cycle number using (a–e) NMC532, (f) NMC622, (g) NMC811, and (h) all three of them cathodes in various electrolytes. Reprinted with permission from Ref. [63] Copyright 2018 IOP Publishing, Ref. [65] Copyright 2019 Springer Nature, Ref. [66] Copyright 2020 Springer Nature, Ref. [67] Copyright 2020 Elsevier, Ref. [68] Copyright 2019 Royal Society of Chemistry, Ref. [69] Copyright 2018 Springer Nature, Ref. [70] Copyright 2020 Springer Nature.

J. R. Dahn's group tested 65 electrolyte mixtures based on an anode-free pouch cell architecture with a high-mass-loading (16 mg cm<sup>-2</sup>, or 3.47 mAh cm<sup>-2</sup>) NMC811 as cathode and a commercial Cu foil as a lithium-free electrode. According to collected total energy delivered above 140 cycles, it showed that only four electrolytes can enhance the energy output over the baseline, and the other electrolytes were uncompetitive [71].

Anode-free pouch cells of Cu || NMC532 using 1 M LiFSI/fluorinated 1,4-dimethoxybutane (FDMB) as electrolyte were evaluated, and the cells can achieve a 80% CR after 100 cycles, which was super than the cells of Cu || NMC622 and Cu || NM811 with same electrolyte (Figure 8h). It should be noted that all the cells above were tested under 100% depth of discharge [70].

### 3.2.2. LFP Cathode

With the high concentration ether-based electrolyte of 4 M LiFSI-DME, the Cu || LFP cell had the first charge/discharge capacities of 148/143 mAh g<sup>-1</sup> and retained the capacity of 85 mAh g<sup>-1</sup> after 50 cycles, that is ~60% CR with an average CE > 99%. Its performance can be even further enhanced by adopting a slow charge and fast discharge protocol. After 100 cycles at a low rate (0.2 mA cm<sup>-2</sup>) charge and high rate (2.0 mA cm<sup>-2</sup>) discharge, the discharge capacity was ~54% of the original value. It was a sizeable increase compared to the cells using the same current density of 0.2 mA cm<sup>-2</sup> for both charge and discharge with a CR of only ~32%. The average CE of the anode-free cells also increased from 98.8% to 99.8% when the cycled protocol was changed (Figure 9a) [72].

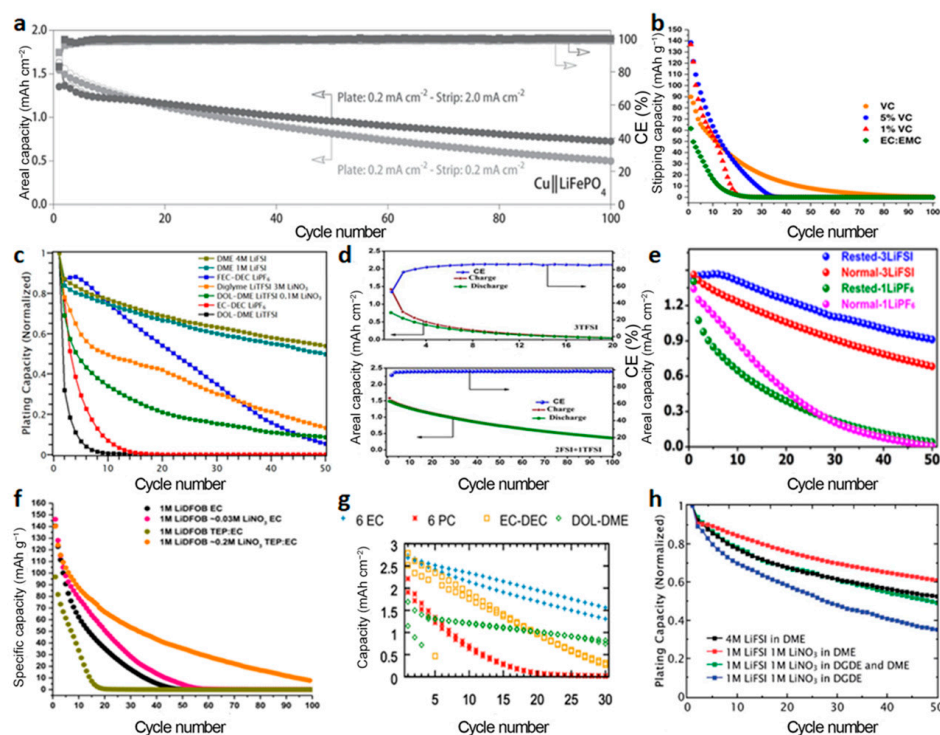


**Figure 9.** Comparison of CR and CE versus cycle number using LFP cathodes and various electrolytes (a–h) [72–79]. Reprinted with permission from Ref. [72] Copyright 2016, John Wiley and Sons; Ref. [74] Copyright 2018 American Chemical Society; Ref. [76] Copyright 2019 American Chemical Society; Ref. [78] Copyright 2019 American Chemical Society; Ref. [79] Copyright 2020 Royal Society of Chemistry.

The influence of VC on the plating/stripping of lithium was investigated using cells of Cu || LFP in a 1.2 M LiPF<sub>6</sub>-EC/EMC electrolyte. It was indicated that increasing the concentration of VC in the electrolyte can boost the cycle life and Coulombic efficiency (Figure 9b) [73].

The Cu || LFP cell in a 4 M LiFSI-DME electrolyte demonstrated the best CR of all tested electrolytes; while the electrodeposited lithium exhibited similar deposition morphology from this electrolyte to the ones from other electrolytes with poor CR. Optical imaging of deposited Li revealed that, even at high specific capacities, the electrolyte with high concentration of LiNO<sub>3</sub> could inhibit dendrite formation (Figure 9c) [74].

Hwang's group reported a dual-salt electrolyte, 2 M LiFSI + 1 M LiTFSI (2FSI + 1TFSI) in DME/DOL (1:1, *v/v*), to compare with the single salt electrolyte of 3 M LiTFSI (3TFSI) in DME/DOL (1:1, *v/v*). A dual-salt electrolyte system can stabilize AFLB with LFP as the cathode and bare Cu as the anode. This battery could retain > 50% of the initial capacity in 50 cycles which by far exceeded the control electrolyte (Figure 9d) [75].

The Cu || LFP cells with electrolyte of 1 M LiPF<sub>6</sub> in EC/DEC (1LiPF<sub>6</sub>) using the "Rested" cycling protocol (before stripping at a high rate, firstly charged at a low rate and the deposited Li was kept rested for 24 h) showed very poor performance. They retained < 30% of the initial capacity after 15 cycles. The battery of Normal-3LiFSI showed a better performance within 50 cycles, with an average CE of 98.03% and retaining 46.70% of its initial discharge capacity. Exceptionally, using the "Rested" cycling protocol, the cycling performance of the Cu || LFP cell with 3 M LiFSI in DOL:DME (3LiFSI) was further improved with an average CE reaching 98.97% and retaining 63.78% of its initial discharge capacity after 50 cycles (Figure 9e) [76].

A baseline carbonate electrolyte, 1 M LiDFOB dissolved in EC:DMC has been developed in AFLB. The Cu || LFP cell containing this electrolyte was achieved over 25 cycles before the capacity was decayed below 20% of the initial capacity. When saturating the

LiDFOB/EC electrolyte with  $\text{LiNO}_3$ , the CEs were further increased to 98% after 10 cycles with an improvement in cycle life. To increase the solubility of  $\text{LiNO}_3$ , TEP was also employed to the electrolyte of  $\sim 0.2$  M ( $\text{LiDFOB LiNO}_3$  TEP:EC). This further improved the performance, with a CE up to 99% after 15 cycles and cycling for 65 cycles before the CR dropped below 20%. The electrolyte of LiDFOB in TEP:EC showed poor performance without  $\text{LiNO}_3$  additive compared to the other investigated electrolytes, with a CE of 62% in the first cycle and a reversible cycle of 13 before the capacity was dropped below 20% of the initial capacity (Figure 9f) [77].

The cells using 1:6 LiTFSI:PC (6 PC) electrolyte lose all capacity within 20 cycles, while for the cells with other electrolytes, the remaining discharge capacities were still high after 30 cycles. The related electrolytes and the CRs after 30 cycles were shown as follows: 1 M LiTFSI in 1:1 EC:DEC (EC-DEC), 8%; 1 M LiTFSI + 0.2 M  $\text{LiNO}_3$  in 1:1 DOL:DME (DOL-DME), 22%; 1:6 LiTFSI:EC (6 EC), 41%. The overall highest capacity loss is observed for DOL-DME electrolytes, where the rapid capacity decay indicated severe electrolyte oxidation (Figure 9g) [78].

Based on the anode-free lithium-ion coin cells, it revealed that the cells with the 1 M LiFSI and 1 M  $\text{LiNO}_3$  in the DME solvent as electrolyte showed the best cycling stability (approximately 34% loss after 50 cycles) compared to electrolytes with different solvents. Once the solvent of DME was replaced by DGDE, the CR was markedly decreased (Figure 9h) [79].

### 3.2.3. Other Cathodes

The  $\text{Cu} \parallel \text{LFP}$  full cells employing 2 M  $\text{LiCF}_3\text{SO}_3$  in DME/DOL as electrolyte with 0.2 M  $\text{LiNO}_3$  as additive failed within 10 cycles. In contrast, the  $\text{Cu} \parallel \text{Li}_2\text{S}$  full cell showed a CR of 51.5% over 100 cycles at a rate of 0.1C with an average Coulombic efficiency of 97.2% over the first 50 cycles (Figure 10) [30].

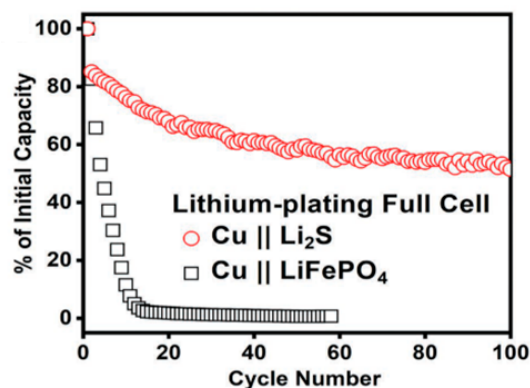


**Figure 10.** Capacity retention of lithium-plating full cells with  $\text{Li}_2\text{S}$  and  $\text{LiFePO}_4$  cathodes. Reprinted with permission from Ref. [30]. Copyright 2018 John Wiley and Sons.

### 3.3. Optimization of the Cycling Protocols

Cycling protocols including charge and discharge current density [25], cut-off voltage [63], temperature [46], external pressure [64,80], etc. are also important for improving the electrochemical performance of AFLBs. These protocols are beneficial to mechanism investigation but may not be suitable for application in real life.

J. R. Dahn's group is the uppermost contributor to the research in this area. Combined with the electrolyte improvement such as the dual-salt usage and concentration tuning, they demonstrated that the different current densities during the charge and discharge process would affect the performance of AFLBs. They found that the rate of charge/discharge current density was much more important compared to their absolute current densities and an asymmetric charge/discharge action played an important role in cells' cycling stability. Similar results were also shown in the previous studies on lithium metal anodes. Then, the effect of discharge depth and lower voltage cut-off were also chosen to examine

the possibility to form an in situ lithium reservoir. The results showed that the optimal lithium reservoir can significantly extend the lifetime of cells within a fixed discharge depth. Finally, they developed an advanced intermittent discharge cycling strategy and made optimization for anode-free lithium metal cells [25].

A brand new “hot formation” method was also presented to improve the long-cycle-ability of Li metal anodes at low temperatures. The capacity of anode-free full cells (Cu | | NMC532) at pressure of 75 kPa was demonstrated to decrease significantly when the operating temperature was changed from 40 °C to room temperature. Different from that at 20 °C, a dense and columnar-like lithium anode would form as the lithium plated at relatively low pressure around 75 kPa and initial 40 °C. Before the room temperature cycling, as “hot formation”, two 40 °C cycles (0.1C charge and 0.5C discharge) were carried out, respectively. They found a significant impact on cycling stability of cells when using LiDFOB/LiBF<sub>4</sub> dual-salt as electrolyte from “hot formation” process. The capacity retention with hot formation can be kept at ~80% for 60 cycles, while only 18 cycles can be maintained without that process. As the applied pressure increased to around 1200 kPa, these cells with the hot formation displayed a capacity retention of 85% upon 100 cycles. Using a high concentration dual salt electrolyte, the “hot formation” strategy was demonstrated to improve cycling stability with an average CE of 99.67% after more than 200 cycles (Figure 11) [81].

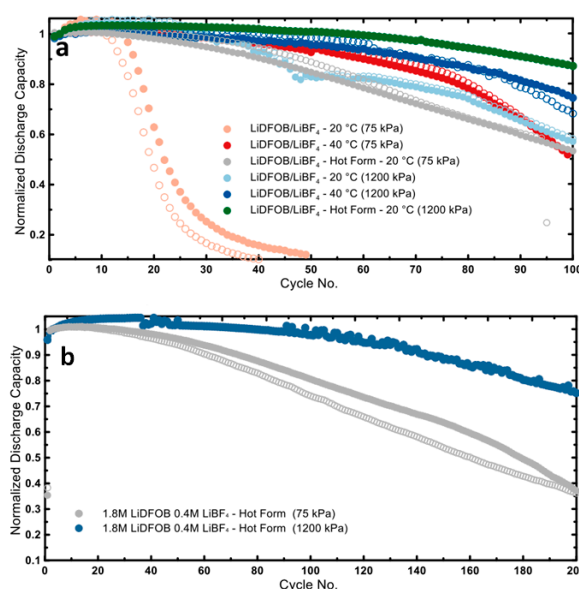


**Figure 11.** (a) Discharge capacity of anode-free cells cycled with or without hot formation protocol (b) Capacity retention of Cu | | NMC532 cells cycled in high concentration electrolyte (1.8 M LiDFOB in 0.4 M LiBF<sub>4</sub> FEC:DEC, 1:2) at room temperature after “hot formation” [81].

#### 4. Future Prospects

To improve the electrochemical performance of AFLB, many approaches have been developed which are reviewed above. The practical application is still limited by the insufficient cycle life which is normally less than 200 cycles with a CR of 80%. Some of the prospects are suggested as follows:

- (1) Separators are always ignored in the previously reported works. Besides coating layers and SEI, separators are important obstructions to prevent mossy and dendritic growth which could lead to short circuits. The optimization of the separator is also essential for prolonging the cycle lifespan.
- (2) The key scientific issues such as the SEI formation and its evolution mechanism, the dynamic performance of lithium ions, as well as the role of the electrolyte functional group desire further probing.

- (3) Most experiments only exist at the laboratory level with coin cells. They help solve problems from the point of mechanism. However, the direct transfer of these strategies to scaled-up pouch cells with the energy density calculation appears not successful in most cases. Much more effort should be devoted to the practical use.

## 5. Conclusions

The anode-free design of lithium is an important milestone for the development of lithium-ion batteries, as it delivers the highest capacity and energy density by eliminating all the anode materials and utilizing the maximum output voltage of the cathode. The elimination of Li during cell manufacture simplifies the cell assembly and improves safety as well as lowers the cost. However, their exploration is still in the elementary stage. The limitation of the cycle life and the heterogeneous lithium deposition are the major obstacles in the practical application. In this review, we compared the energy density of the anode-free cells paired with various cathodes/hybrid cathodes, summarized the strategies for performance improvement with the classification from the perspective of cathodes in each strategy part, as well as provided an overview of the main advantages and limitations and outlined the prospects. We anticipate this review could be a useful handbook for research in AFLBs and offer inspiration for further novel designs for enhancing the cycling performance of AFLBs.

**Author Contributions:** Writing—original draft preparation, P.Z.; review and editing, D.Z., Z.T., Y.L., J.P. and Y.T.; supervision, Y.L., H.G. and F.H.; funding acquisition, Z.T., Y.L. and J.P. All authors have read and agreed to the published version of the manuscript.

**Funding:** This research is financially supported by Guangdong Science and Technology Department (Grant Number: 2022A1515110877), Bureau of Science and Technology of Jiangmen Municipality (Grant Number: 2220002000335), National Nature Science Foundation of China (No. 22209199), and Taishan Industry Leading Talent Project (NO. tscx202211146).

**Data Availability Statement:** No new data were created or analyzed in this study. Data sharing is not applicable to this article.

**Conflicts of Interest:** The authors declare no conflict of interest.

## References

1. Dunn, B.; Kamath, H.; Tarascon, J.M. Electrical energy storage for the grid: A battery of choices. *Science* **2011**, *334*, 928–935. [[CrossRef](#)] [[PubMed](#)]
2. Goodenough, J.B.; Kim, Y. Challenges for rechargeable Li batteries. *Chem. Mater.* **2010**, *22*, 587–603. [[CrossRef](#)]
3. Tarascon, J.M.; Armand, M. Issues and challenges facing rechargeable lithium batteries. *Nature* **2001**, *414*, 359–367. [[CrossRef](#)] [[PubMed](#)]
4. Lin, D.C.; Liu, Y.Y.; Cui, Y. Reviving the lithium metal anode for high-energy batteries. *Nat. Nanotechnol.* **2017**, *12*, 194–206. [[CrossRef](#)] [[PubMed](#)]
5. Albertus, P.; Babinec, S.; Litzelman, S.; Newman, A. Status and challenges in enabling the lithium metal electrode for high-energy and low-cost rechargeable batteries. *Nat. Energy* **2017**, *3*, 16–21. [[CrossRef](#)]
6. Liu, J.; Bao, Z.N.; Cui, Y.; Dufek, E.J.; Goodenough, J.B.; Khalifah, P.; Li, Q.Y.; Liaw, B.Y.; Liu, P.; Manthiram, A.; et al. Pathways for practical high-energy long-cycling lithium metal batteries. *Nat. Energy* **2019**, *4*, 180–186. [[CrossRef](#)]
7. Schmuck, R.; Wagner, R.; Horpel, G.; Placke, T.; Winter, M. Performance and cost of materials for lithium-based rechargeable automotive batteries. *Nat. Energy* **2018**, *3*, 267–278. [[CrossRef](#)]
8. Heubner, C.; Maletti, S.; Auer, H.; Hüttel, J.; Voigt, K.; Lohrberg, O.; Nikolowski, K.; Partsch, M.; Michaelis, A. From lithium-metal toward anode-free solid-state batteries: Current developments, issues, and challenges. *Adv. Funct. Mater.* **2021**, *31*, 2106608. [[CrossRef](#)]
9. Woo, J.-J.; Maroni, V.A.; Liu, G.; Vaughey, J.T.; Gosztola, D.J.; Amine, K.; Zhang, Z. Symmetrical impedance study on inactivation induced degradation of lithium electrodes for batteries beyond lithium-ion. *J. Electrochem. Soc.* **2014**, *161*, A827–A830. [[CrossRef](#)]
10. Nanda, S.; Gupta, A.; Manthiram, A. Anode-free full cells: A pathway to high-energy density lithium-metal batteries. *Adv. Energy Mater.* **2020**, *11*, 2000804. [[CrossRef](#)]
11. Cui, S.; Zhai, P.; Yang, W.; Wei, Y.; Xiao, J.; Deng, L.; Gong, Y. Large-scale modification of commercial copper foil with lithiophilic metal layer for Li metal battery. *Small* **2020**, *16*, e1905620. [[CrossRef](#)]
12. Tong, Z.; Bazri, B.; Hu, S.F.; Liu, R.S. Interfacial chemistry in anode-free batteries: Challenges and strategies. *J. Mater. Chem. A* **2021**, *9*, 7396–7406. [[CrossRef](#)]

13. Hagos, T.M.; Bezabh, H.K.; Huang, C.-J.; Jiang, S.-K.; Su, W.-N.; Hwang, B.J. A powerful protocol based on anode-free cells combined with various analytical techniques. *Acc. Chem. Res.* **2021**, *54*, 4474–4485. [[CrossRef](#)] [[PubMed](#)]
14. Shao, A.; Tang, X.; Zhang, M.; Bai, M.; Ma, Y. Challenges, strategies, and prospects of the anode-free lithium metal batteries. *Adv. Energy Sustain. Res.* **2022**, *3*, 2100197. [[CrossRef](#)]
15. Tian, Y.; An, Y.; Wei, C.; Jiang, H.; Xiong, S.; Feng, J.; Qian, Y. Recently advances and perspectives of anode-free rechargeable batteries. *Nano Energy* **2020**, *78*, 105344. [[CrossRef](#)]
16. Xie, Z.; Wu, Z.; An, X.; Yue, X.; Wang, J.; Abudula, A.; Guan, G. Anode-free rechargeable lithium metal batteries: Progress and prospects. *Energy Storage Mater.* **2020**, *32*, 386–401. [[CrossRef](#)]
17. Jo, C.H.; Sohn, K.S.; Myung, S.T. Feasible approaches for anode-free lithium-metal batteries as next generation energy storage systems. *Energy Storage Mater.* **2023**, *57*, 471–496. [[CrossRef](#)]
18. Wu, B.L.; Chen, C.G.; Rajmakers, L.H.J.; Liu, J.; Danilov, D.L.; Notten, P.H.L. Li-growth and SEI engineering for anode-free Li-metal rechargeable batteries: A review of current advances. *Energy Storage Mater.* **2023**, *57*, 508–539. [[CrossRef](#)]
19. Louli, A.J.; Eldesoky, A.; deGooyer, J.; Coon, M.; Aiken, C.P.; Simunovic, Z.; Metzger, M.; Dahn, J.R. Different positive electrodes for anode-free lithium metal cells. *J. Electrochem. Soc.* **2022**, *169*, 040517. [[CrossRef](#)]
20. Lin, L.; Qin, K.; Zhang, Q.; Gu, L.; Suo, L.; Hu, Y.S.; Li, H.; Huang, X.; Chen, L. Li-rich  $\text{Li}_2[\text{Ni}_{0.8}\text{Co}_{0.1}\text{Mn}_{0.1}]\text{O}_2$  for anode-free lithium metal batteries. *Angew. Chem. Int. Ed. Engl.* **2021**, *60*, 8289–8296. [[CrossRef](#)]
21. Qiao, Y.; Yang, H.; Chang, Z.; Deng, H.; Li, X.; Zhou, H. A high-energy-density and long-life initial-anode-free lithium battery enabled by a  $\text{Li}_2\text{O}$  sacrificial agent. *Nat. Energy* **2021**, *6*, 653–662. [[CrossRef](#)]
22. Assegie, A.A.; Chung, C.C.; Tsai, M.C.; Su, W.N.; Chen, C.W.; Hwang, B.J. Multilayer-graphene-stabilized lithium deposition for anode-free lithium-metal batteries. *Nanoscale* **2019**, *11*, 2710–2720. [[CrossRef](#)] [[PubMed](#)]
23. Hagos, T.T.; Thirumalraj, B.; Huang, C.J.; Abrha, L.H.; Hagos, T.M.; Berhe, G.B.; Bezabh, H.K.; Cherng, J.; Chiu, S.F.; Su, W.N.; et al. Locally concentrated  $\text{LiPF}_6$  in a carbonate-based electrolyte with fluoroethylene carbonate as a diluent for anode-free lithium metal batteries. *ACS Appl. Mater. Interfaces* **2019**, *11*, 9955–9963. [[CrossRef](#)] [[PubMed](#)]
24. Sahalie, N.A.; Assegie, A.A.; Su, W.-N.; Wondimkun, Z.T.; Jote, B.A.; Thirumalraj, B.; Huang, C.-J.; Yang, Y.-W.; Hwang, B.-J. Effect of bifunctional additive potassium nitrate on performance of anode free lithium metal battery in carbonate electrolyte. *J. Power Sources* **2019**, *437*, 226912. [[CrossRef](#)]
25. Louli, A.J.; Coon, M.; Genovese, M.; deGooyer, J.; Eldesoky, A.; Dahn, J.R. Optimizing cycling conditions for anode-free lithium metal cells. *J. Electrochem. Soc.* **2021**, *168*, 020515. [[CrossRef](#)]
26. Lee, Y.-G.; Fujiki, S.; Jung, C.; Suzuki, N.; Yashiro, N.; Omoda, R.; Ko, D.-S.; Shiratsuchi, T.; Sugimoto, T.; Ryu, S.; et al. High-energy long-cycling all-solid-state lithium metal batteries enabled by silver-carbon composite anodes. *Nat. Energy* **2020**, *5*, 299–308. [[CrossRef](#)]
27. Su, L.; Charalambous, H.; Cui, Z.; Manthiram, A. High-efficiency, anode-free lithium-metal batteries with a close-packed homogeneous lithium morphology. *Energy Environ. Sci.* **2022**, *15*, 843–854. [[CrossRef](#)]
28. Tu, Z.; Zachman, M.J.; Choudhury, S.; Khan, K.A.; Zhao, Q.; Kourkoutis, L.F.; Archer, L.A. Stabilizing protic and aprotic liquid electrolytes at high-bandgap oxide interphases. *Chem. Mater.* **2018**, *30*, 5655–5662. [[CrossRef](#)]
29. Cheng, H.; Gao, C.; Cai, N.; Wang, M. Ag coated 3D-Cu foam as a lithiophilic current collector for enabling  $\text{Li}_2\text{S}$ -based anode-free batteries. *Chem. Commun.* **2021**, *57*, 3708–3711. [[CrossRef](#)]
30. Nanda, S.; Gupta, A.; Manthiram, A. A lithium-sulfur cell based on reversible lithium deposition from a  $\text{Li}_2\text{S}$  cathode host onto a hostless-anode substrate. *Adv. Energy Mater.* **2018**, *8*, 1801556. [[CrossRef](#)]
31. Chen, J.; Xiang, J.; Chen, X.; Yuan, L.; Li, Z.; Huang, Y.  $\text{Li}_2\text{S}$ -based anode-free full batteries with modified Cu current collector. *Energy Storage Mater.* **2020**, *30*, 179–186. [[CrossRef](#)]
32. Nanda, S.; Bhargav, A.; Manthiram, A. Anode-free, lean-electrolyte lithium-sulfur batteries enabled by tellurium-stabilized lithium deposition. *Joule* **2020**, *4*, 1121–1135. [[CrossRef](#)]
33. Liu, S.; Zhang, X.Y.; Li, R.S.; Gao, L.B.; Luo, J.Y. Dendrite-free Li metal anode by lowering deposition interface energy with  $\text{Cu}_{99}\text{Zn}$  alloy coating. *Energy Storage Mater.* **2018**, *14*, 143–148. [[CrossRef](#)]
34. Lin, L.; Qin, K.; Li, M.; Hu, Y.-s.; Li, H.; Huang, X.; Chen, L.; Suo, L. Spinel-related  $\text{Li}_2\text{Ni}_{0.5}\text{Mn}_{1.5}\text{O}_4$  cathode for 5-V anode-free lithium metal batteries. *Energy Storage Mater.* **2022**, *45*, 821–827. [[CrossRef](#)]
35. Wu, Y.; Shen, B.; Zhu, Z.; He, Y.; Wei, Z.; Wei, J.; Jiang, H.; Hu, Y.; Li, C. Multifunctional lithium compensation agent based on carbon edges catalysis and its application in anode-free lithium batteries. *Chem. Eng. J.* **2023**, *458*, 141411. [[CrossRef](#)]
36. Zhang, S.S.; Fan, X.L.; Wang, C.S. An in-situ enabled lithium metal battery by plating lithium on a copper current collector. *Electrochem. Commun.* **2018**, *89*, 23–26. [[CrossRef](#)]
37. Park, S.W.; Choi, H.J.; Yoo, Y.; Lim, H.D.; Park, J.W.; Lee, Y.J.; Ha, Y.C.; Lee, S.M.; Kim, B.G. Stable cycling of all-solid-state batteries with sacrificial cathode and lithium-free indium layer. *Adv. Funct. Mater.* **2021**, *32*, 2108203. [[CrossRef](#)]
38. Pei, A.; Zheng, G.; Shi, F.; Li, Y.; Cui, Y. Nanoscale nucleation and growth of electrodeposited lithium metal. *Nano Lett.* **2017**, *17*, 1132–1139. [[CrossRef](#)]
39. Umh, H.N.; Park, J.; Yeo, J.; Jung, S.; Nam, I.; Yi, J. Lithium metal anode on a copper dendritic superstructure. *Electrochem. Commun.* **2019**, *99*, 27–31. [[CrossRef](#)]
40. Chen, J.; Dai, L.; Hu, P.; Li, Z. Facile one-step heat treatment of Cu foil for stable anode-free Li metal batteries. *Molecules* **2023**, *28*, 548. [[CrossRef](#)]

41. Lo, C.A.; Chang, C.C.; Tsai, Y.W.; Jiang, S.K.; Hwang, B.J.; Mou, C.Y.; Wu, H.L. Regulated Li electrodeposition behavior through mesoporous silica thin film in anode-free lithium metal batteries. *ACS Appl. Energy Mater.* **2021**, *4*, 5132–5142. [[CrossRef](#)]
42. Weldeyohannes, H.H.; Abrha, L.H.; Nikodimos, Y.; Shitaw, K.N.; Hagos, T.M.; Huang, C.-J.; Wang, C.-H.; Wu, S.-H.; Su, W.-N.; Hwang, B.J. Guiding lithium-ion flux to avoid cell's short circuit and extend cycle life for an anode-free lithium metal battery. *J. Power Sources* **2021**, *506*, 230204. [[CrossRef](#)]
43. Abrha, L.H.; Zegeye, T.A.; Hagos, T.T.; Sutiono, H.; Hagos, T.M.; Berhe, G.B.; Huang, C.-J.; Jiang, S.-K.; Su, W.-N.; Yang, Y.-W.; et al.  $\text{Li}_7\text{La}_{2.75}\text{Ca}_{0.25}\text{Zr}_{1.75}\text{Nb}_{0.25}\text{O}_{12}@\text{LiClO}_4$  composite film derived solid electrolyte interphase for anode-free lithium metal battery. *Electrochim. Acta* **2019**, *325*, 134825. [[CrossRef](#)]
44. Sahalie, N.A.; Wondimkun, Z.T.; Su, W.-N.; Weret, M.A.; Fenta, F.W.; Berhe, G.B.; Huang, C.-J.; Hsu, Y.-C.; Hwang, B.J. Multifunctional properties of  $\text{Al}_2\text{O}_3$ /polyacrylonitrile composite coating on Cu to suppress dendritic growth in anode-free Li-metal battery. *ACS Appl. Energy Mater.* **2020**, *3*, 7666–7679. [[CrossRef](#)]
45. Wondimkun, Z.T.; Beyene, T.T.; Weret, M.A.; Sahalie, N.A.; Huang, C.-J.; Thirumalraj, B.; Jote, B.A.; Wang, D.; Su, W.-N.; Wang, C.-H.; et al. Binder-free ultra-thin graphene oxide as an artificial solid electrolyte interphase for anode-free rechargeable lithium metal batteries. *J. Power Sources* **2020**, *450*, 227589. [[CrossRef](#)]
46. Abrha, L.H.; Nikodimos, Y.; Weldeyohannes, H.H.; Hagos, T.T.; Wang, D.Y.; Huang, C.J.; Jiang, S.K.; Wu, S.H.; Su, W.N.; Tsai, M.C.; et al. Effects of a thermally electrochemically activated  $\beta$ -PVDF fiber on suppression of Li dendrite growth for anode-free batteries. *ACS Appl. Energy Mater.* **2021**, *4*, 3240–3248. [[CrossRef](#)]
47. Wondimkun, Z.T.; Tegegne, W.A.; Jiang, S.K.; Huang, C.J.; Sahalie, N.A.; Weret, M.A.; Hsu, J.Y.; Hsieh, P.L.; Huang, Y.S.; Wu, S.H.; et al. Highly-lithiophilic  $\text{Ag@PDA-GO}$  film to suppress dendrite formation on Cu substrate in anode-free lithium metal batteries. *Energy Storage Mater.* **2021**, *35*, 334–344. [[CrossRef](#)]
48. Temesgen, N.T.; Tegegne, W.A.; Shitaw, K.N.; Fenta, F.W.; Nikodimos, Y.; Taklu, B.W.; Jiang, S.-K.; Huang, C.-J.; Wu, S.-H.; Su, W.-N.; et al. Mitigating dendrite formation and electrolyte decomposition via functional double layers coating on copper current collector in anode-free lithium metal battery. *J. Taiwan Inst. Chem. Eng.* **2021**, *128*, 87–97. [[CrossRef](#)]
49. Wang, C.; Liu, M.; Thijs, M.; Ooms, F.G.B.; Ganapathy, S.; Wagemaker, M. High dielectric barium titanate porous scaffold for efficient Li metal cycling in anode-free cells. *Nat. Commun.* **2021**, *12*, 6536. [[CrossRef](#)]
50. Lin, L.; Suo, L.; Hu, Y.-s.; Li, H.; Huang, X.; Chen, L. Epitaxial induced plating current-collector lasting lifespan of anode-free lithium metal battery. *Adv. Energy Mater.* **2021**, *11*, 2003709. [[CrossRef](#)]
51. Assegie, A.A.; Cheng, J.H.; Kuo, L.M.; Su, W.N.; Hwang, B.J. Polyethylene oxide film coating enhances lithium cycling efficiency of an anode-free lithium-metal battery. *Nanoscale* **2018**, *10*, 6125–6138. [[CrossRef](#)]
52. Liu, H.; Yue, X.; Xing, X.; Yan, Q.; Huang, J.; Petrova, V.; Zhou, H.; Liu, P. A scalable 3D lithium metal anode. *Energy Storage Mater.* **2019**, *16*, 505–511. [[CrossRef](#)]
53. Chen, W.; Salvatierra, R.V.; Ren, M.; Chen, J.; Stanford, M.G.; Tour, J.M. Laser-induced silicon oxide for anode-free lithium metal batteries. *Adv. Mater.* **2020**, *32*, e2002850. [[CrossRef](#)]
54. Kang, T.; Zhao, J.; Guo, F.; Zheng, L.; Mao, Y.; Wang, C.; Zhao, Y.; Zhu, J.; Qiu, Y.; Shen, Y.; et al. Dendrite-free lithium anodes enabled by a commonly used copper antirusting agent. *ACS Appl. Mater. Interfaces* **2020**, *12*, 8168–8175. [[CrossRef](#)] [[PubMed](#)]
55. Chen, J.; Li, Q.; Pollard, T.P.; Fan, X.; Borodin, O.; Wang, C. Electrolyte design for Li metal-free Li batteries. *Mater. Today* **2020**, *39*, 118–126. [[CrossRef](#)]
56. Li, Q.; Pan, H.Y.; Li, W.J.; Wang, Y.; Wang, J.Y.; Zheng, J.Y.; Yu, X.Q.; Li, H.; Chen, L.Q. Homogeneous interface conductivity for lithium dendrite-free anode. *ACS Energy Lett.* **2018**, *3*, 2259–2266. [[CrossRef](#)]
57. Tamwattana, O.; Park, H.; Kim, J.; Hwang, I.; Yoon, G.; Hwang, T.-h.; Kang, Y.-S.; Park, J.; Meethong, N.; Kang, K. High-dielectric polymer coating for uniform lithium deposition in anode-free lithium batteries. *ACS Energy Lett.* **2021**, *6*, 4416–4425. [[CrossRef](#)]
58. Neudecker, B.J.; Dudney, N.J.; Bates, J.B. "Lithium-free" thin-film battery with in situ plated Li anode. *J. Electrochem. Soc.* **2000**, *147*, 517–523. [[CrossRef](#)]
59. Zhang, S.S.; Fan, X.; Wang, C. A tin-plated copper substrate for efficient cycling of lithium metal in an anode-free rechargeable lithium battery. *Electrochim. Acta* **2017**, *258*, 1201–1207. [[CrossRef](#)]
60. Huang, W.Z.; Zhao, C.Z.; Wu, P.; Yuan, H.; Feng, W.E.; Liu, Z.Y.; Lu, Y.; Sun, S.; Fu, Z.H.; Hu, J.K.; et al. Anode-free solid-state lithium batteries: A review. *Adv. Energy Mater.* **2022**, *12*, 2201044. [[CrossRef](#)]
61. Hagos, T.M.; Berhe, G.B.; Hagos, T.T.; Bezabh, H.K.; Abrha, L.H.; Beyene, T.T.; Huang, C.-J.; Yang, Y.-W.; Su, W.-N.; Dai, H.; et al. Dual electrolyte additives of potassium hexafluorophosphate and tris (trimethylsilyl) phosphite for anode-free lithium metal batteries. *Electrochim. Acta* **2019**, *316*, 52–59. [[CrossRef](#)]
62. Hagos, T.T.; Su, W.-N.; Huang, C.-J.; Thirumalraj, B.; Chiu, S.-F.; Abrha, L.H.; Hagos, T.M.; Bezabh, H.K.; Berhe, G.B.; Tegegne, W.A.; et al. Developing high-voltage carbonate-ether mixed electrolyte via anode-free cell configuration. *J. Power Sources* **2020**, *461*, 228053. [[CrossRef](#)]
63. Genovese, M.; Louli, A.J.; Weber, R.; Hames, S.; Dahn, J.R. Measuring the coulombic efficiency of lithium metal cycling in anode-free lithium metal batteries. *J. Electrochem. Soc.* **2018**, *165*, A3321–A3325. [[CrossRef](#)]
64. Louli, A.J.; Genovese, M.; Weber, R.; Hames, S.G.; Logan, E.R.; Dahn, J.R. Exploring the impact of mechanical pressure on the performance of anode-free lithium metal cells. *J. Electrochem. Soc.* **2019**, *166*, A1291–A1299. [[CrossRef](#)]
65. Weber, R.; Genovese, M.; Louli, A.J.; Hames, S.; Martin, C.; Hill, I.G.; Dahn, J.R. Long cycle life and dendrite-free lithium morphology in anode-free lithium pouch cells enabled by a dual-salt liquid electrolyte. *Nat. Energy* **2019**, *4*, 683–689. [[CrossRef](#)]

66. Louli, A.J.; Eldesoky, A.; Weber, R.; Genovese, M.; Coon, M.; deGooyer, J.; Deng, Z.; White, R.T.; Lee, J.; Rodgers, T.; et al. Diagnosing and correcting anode-free cell failure via electrolyte and morphological analysis. *Nat. Energy* **2020**, *5*, 693–702. [[CrossRef](#)]
67. Jote, B.A.; Beyene, T.T.; Sahalie, N.A.; Weret, M.A.; Olbassa, B.W.; Wondimkun, Z.T.; Berhe, G.B.; Huang, C.-J.; Su, W.-N.; Hwang, B.J. Effect of diethyl carbonate solvent with fluorinated solvents as electrolyte system for anode free battery. *J. Power Sources* **2020**, *461*, 228102. [[CrossRef](#)]
68. Alvarado, J.; Schroeder, M.A.; Pollard, T.P.; Wang, X.; Lee, J.Z.; Zhang, M.; Wynn, T.; Ding, M.; Borodin, O.; Meng, Y.S.; et al. Bisalt ether electrolytes: A pathway towards lithium metal batteries with Ni-rich cathodes. *Energy Environ. Sci.* **2019**, *12*, 780–794. [[CrossRef](#)]
69. Fan, X.; Chen, L.; Borodin, O.; Ji, X.; Chen, J.; Hou, S.; Deng, T.; Zheng, J.; Yang, C.; Liou, S.C.; et al. Non-flammable electrolyte enables Li-metal batteries with aggressive cathode chemistries. *Nat. Nanotechnol.* **2018**, *13*, 715–722. [[CrossRef](#)]
70. Yu, Z.; Wang, H.; Kong, X.; Huang, W.; Tsao, Y.; Mackanic, D.G.; Wang, K.; Wang, X.; Huang, W.; Choudhury, S.; et al. Molecular design for electrolyte solvents enabling energy-dense and long-cycling lithium metal batteries. *Nat. Energy* **2020**, *5*, 526–533. [[CrossRef](#)]
71. Eldesoky, A.; Louli, A.J.; Benson, A.; Dahn, J.R. Cycling performance of NMC811 anode-free pouch cells with 65 different electrolyte formulations. *J. Electrochem. Soc.* **2021**, *168*, 120508. [[CrossRef](#)]
72. Qian, J.; Adams, B.D.; Zheng, J.; Xu, W.; Henderson, W.A.; Wang, J.; Bowden, M.E.; Xu, S.; Hu, J.; Zhang, J.-G. Anode-free rechargeable lithium metal batteries. *Adv. Funct. Mater.* **2016**, *26*, 7094–7102. [[CrossRef](#)]
73. Brown, Z.L.; Jurng, S.; Lucht, B.L. Investigation of the lithium solid electrolyte interphase in vinylene carbonate electrolytes using Cu | LiFePO<sub>4</sub> cells. *J. Electrochem. Soc.* **2017**, *164*, A2186–A2189. [[CrossRef](#)]
74. Rodriguez, R.; Loeffler, K.E.; Edison, R.A.; Stephens, R.M.; Dolocan, A.; Heller, A.; Mullins, C.B. Effect of the electrolyte on the cycling efficiency of lithium-limited cells and their morphology studied through in situ optical imaging. *ACS Appl. Energy Mater.* **2018**, *1*, 5830–5835. [[CrossRef](#)]
75. Beyene, T.T.; Bezabh, H.K.; Weret, M.A.; Hagos, T.M.; Huang, C.J.; Wang, C.H.; Su, W.N.; Dai, H.; Hwang, B.J. Concentrated dual-salt electrolyte to stabilize Li metal and increase cycle life of anode free Li-metal batteries. *J. Electrochem. Soc.* **2019**, *166*, A1501–A1509. [[CrossRef](#)]
76. Beyene, T.T.; Jote, B.A.; Wondimkun, Z.T.; Olbassa, B.W.; Huang, C.J.; Thirumalraj, B.; Wang, C.H.; Su, W.N.; Dai, H.; Hwang, B.J. Effects of concentrated salt and resting protocol on solid electrolyte interface formation for improved cycle stability of anode-free lithium metal batteries. *ACS Appl. Mater. Interfaces* **2019**, *11*, 31962–31971. [[CrossRef](#)] [[PubMed](#)]
77. Brown, Z.L.; Heiskanen, S.; Lucht, B.L. Using triethyl phosphate to increase the solubility of LiNO<sub>3</sub> in carbonate electrolytes for improving the performance of the lithium metal anode. *J. Electrochem. Soc.* **2019**, *166*, A2523–A2527. [[CrossRef](#)]
78. Nilsson, V.; Kotronia, A.; Lacey, M.; Edström, K.; Johansson, P. Highly concentrated LiTFSI-EC electrolytes for lithium metal batteries. *ACS Appl. Energy Mater.* **2019**, *3*, 200–207. [[CrossRef](#)]
79. Rodriguez, R.; Edison, R.A.; Stephens, R.M.; Sun, H.-H.; Heller, A.; Mullins, C.B. Separator-free and concentrated LiNO<sub>3</sub> electrolyte cells enable uniform lithium electrodeposition. *J. Mater. Chem. A* **2020**, *8*, 3999–4006. [[CrossRef](#)]
80. Zhou, C.; Samson, A.J.; Garakani, M.A.; Thangadurai, V. Communication—Anode-free lithium metal batteries: A case study of compression effects on coin cell performance. *J. Electrochem. Soc.* **2021**, *168*, 060532. [[CrossRef](#)]
81. Genovese, M.; Louli, A.J.; Weber, R.; Martin, C.; Taskovic, T.; Dahn, J.R. Hot formation for improved low temperature cycling of anode-free lithium metal batteries. *J. Electrochem. Soc.* **2019**, *166*, A3342–A3347. [[CrossRef](#)]

**Disclaimer/Publisher’s Note:** The statements, opinions and data contained in all publications are solely those of the individual author(s) and contributor(s) and not of MDPI and/or the editor(s). MDPI and/or the editor(s) disclaim responsibility for any injury to people or property resulting from any ideas, methods, instructions or products referred to in the content.